The origins of Antarctic rock glaciers: periglacial or glacial features?

Mauro Guglielmin,[1]* Stefano Ponti[1] and Emanuele Forte[2]
[1] Department of Theoretical and Applied Sciences, Insubria University, Via Dunant, 3, Varese, Italy
[2] Department of Mathematics and Geosciences, University of Trieste, via Weiss, 22, 34128 Trieste, Italy

Accepted 8 December 2017

*Correspondence to: Mauro Guglielmin, Department of Theoretical and Applied Sciences, Insubria University, Via Dunant, 3, Varese, Italy. E-mail: mauro.guglielmin@uninsubria.it

ABSTRACT: In extensively glaciarized permafrost areas such as Northern Victoria Land, rock glaciers are quite common and are considered postglacial cryotic landforms. This paper reveals that two rock glaciers in Northern Victoria Land (at Adélie Cove and Strandline) that are located close to the Italian Antarctic Station (Mario Zucchelli Station) should have the same origin, although they were previously mapped as Holocene periglacial landforms and subsequently considered ice-cored and ice-cemented rock glaciers, respectively. In fact, by integrating different geophysical investigations and borehole stratigraphy, we show that both landforms have similar internal structures and cores of buried glacier ice. Therefore, this kind of rock glacier is possibly related to the long-term creep of buried ice rather than to permafrost creep alone. This interpretation can be extended to the larger part of the features mapped as rock glaciers in Antarctica.

In addition, a high-reflective horizon sub-parallel to the topographic surface was detected in Ground Probing Radar (GPR) data over a large part of the study area. Combining all the available information, we conclude that it cannot be straightforwardly interpreted as the base of the active layer but rather represents the top of a cryo-lithological unit characterized by ice lenses within sediments that could be interpreted as the transition zone between the active layer and the long-term permafrost table. More generally, knowledge of the subsurface ice content and, in particular, the occurrence of massive ice and its depth is crucial to make realistic and affordable forecasts regarding thermokarst development and related feedbacks involving GHG emissions, especially in the case of cryosoils rich in carbon content.

KEYWORDS: geophysical soundings; Antarctica; glacial and periglacial geomorphology; rock glaciers; permafrost; GPR; ERT

Introduction

Rock glaciers are masses of coarse angular debris that display steep fronts and a system of transverse surface ridges and furrows, indicating a downward flow movement (Capps Jr, 1910; Wahrhaftig and Cox, 1959). Rock glaciers are widespread geomorphological features throughout the periglacial areas of both the Southern and Northern Hemispheres (Azócar and Brenning, 2010; Lilleøren and Etzelmüller, 2011; Kellerer-Pirklbauer *et al.*, 2012; Seppi *et al.*, 2012; Janke *et al.*, 2015; Sattler *et al.*, 2016), including Antarctica (Hassinger and Mayewski, 1983; Humlum 1998; Serrano and López-Martínez, 2000; Swanger *et al.*, 2010; López-Martínez *et al.*, 2012; Vieira *et al.*, 2012; Bockheim, 2014). Despite their widespread distribution and relevance, knowledge of their internal structures, ice contents and ice types remains limited. Only a few rock glaciers have been drilled, including the Galena Creek rock glacier (Clark *et al.*, 1996) in North America, the Choapa Valley in the Chilean Andes (Monnier and Kinnard, 2013), the Foscagno rock glacier (Guglielmin *et al.*, 2001; Guglielmin, 2004) and Lazaun rock glacier (Krainer *et al.*, 2015) in the Italian Alps, and Gruben, Murtel, Muragl and Pontresina-Schafberg (Haeberli, 1985; Arenson *et al.*, 2002; Haeberli *et al.*, 2006) in the Swiss Alps. In Antarctica, to the best of our knowledge when submitting this paper, only the Tumbledown Crags rock glacier on James Ross Island has been drilled (at two boreholes) (Fukui *et al.*, 2008). Even less known are the natural exposures of rock glacier internal structures, as reported, for example, by Strelin and Sone (1998) and Ribolini *et al.* (2007). The internal structures of some rock glaciers were investigated through geophysical electrical soundings (especially vertical DC soundings in the past and, more recently, by means of electrical resistivity tomography (ERT) (Haeberli, 1985; King *et al.*, 1987; Evin and Fabre, 1990; Guglielmin *et al.*, 1994, 1997; Hauck, 2001; Hauck *et al.*, 2001; Maurer and Hauck, 2007; Ribolini *et al.*, 2007, 2010) and ground penetrating radar (GPR) (Berthling *et al.*, 2000; Lehmann and Green, 2000; Degenhardt *et al.*, 2003; Fukui *et al.*, 2007; Hausmann *et al.*, 2007; Monnier *et al.*, 2008; Degenhardt Jr., 2009; Leopold *et al.*, 2011; Merz *et al.*, 2015; Hartl *et al.*, 2016). A comprehensive review of several geophysical techniques applied to detect massive sub-surficial ice was reported by Yoshikawa *et al.* (2006).

Moreover, knowledge of the internal structures of rock glaciers can be very helpful or even essential for assessing the

origins of such landforms and their relationships with past and current climate (i.e. Colucci *et al.*, 2016). Indeed, a correct description of the inner structure provides the information that is required to understand and forecast the possible different ways in which a rock glacier responds to environmental and climate changes at different scales.

As suggested by Haeberli (2000), in areas with continental climates where surface ice interacts with periglacial and subglacial permafrost, complex mixtures of buried surface ice and ice formed directly into the ground can occur, and all transitions from *debris-covered polythermal or cold glaciers* to *ice-cored moraines* and *deep-seated creep of perennially frozen sediments* are possible.

Continental Antarctica is probably the best example in which these complex conditions can be found and therefore is mandatory to investigate the compositions, the stratigraphies and structures of rock glaciers and understand the evolution of their landscapes and their sensitivity to climate change.

Although Continental Antarctica and the Ross Sea region in particular, remain among the few areas on the planet over which air warming has not occurred (Doran *et al.*, 2002; Guglielmin and Cannone, 2012; Guglielmin *et al.*, 2014; Turner *et al.*, 2014), several pieces of evidence of rapid landscape changes have been detected in the last 10 years, including fluvial erosion and the thermokarst phenomena in the Dry Valleys (Fountain *et al.*, 2014). In contrast, in the more glaciated Northern Victoria Land, only a small amount of evidence of climatic-related landscape changes has been detected (Guglielmin *et al.*, 2009).

If future climatic scenarios (IPCC, 2013) are confirmed, the rates of landscape changes should abruptly increase even in this part of the planet, with important consequences for ecosystem preservation (Guglielmin *et al.*, 2014) and even for the conservation of existing human infrastructures (Silva Busso and Yermolin, 2017).

The main aims of the paper are (a) to understand and image the internal structure and the ice type occurring in two rock glaciers of Northern Victoria Land through different integrated geophysical investigations and core stratigraphy, and (b) to understand the Antarctic rock glaciers' origins and their relationships with the surrounding glacial evolution.

Study area

The study area is located along the coast close to the Italian Antarctic Station 'Mario Zucchelli' (74°42′S–164°60′E) between Tethys Bay to the north and Adélie Cove to the south (Figure 1) in Northern Victoria Land, Continental Antarctica. This area is characterized by large ice-free areas where the bedrock, which is composed mainly of Ordovician granite, is generally covered by discontinuous and thin tills that can be referred to two different glacial drifts informally named TN I and TN II (Baroni, 1987; Baroni and Orombelli, 1987; Orombelli *et al.*, 1990). More rarely, there are active scree slope and beach deposits. The first geomorphological map of the area, at a scale of 1:20 000 (Baroni, 1987), described the main glacial and periglacial landforms such as rock glaciers occurring along the coast of Adélie Cove and Tethys Bay (Figure 1).

In detail, in this paper, we analyse the rock glacier (ST) located at Tethys Bay close to the northern margin of the Strandline glacier and the rock glacier located on the southern side of Adélie Cove (AD) (Figure 2).

The ST rock glacier is a spatulate rock glacier according to Baroni (1987), is 120 m long and 590 m wide and is developed between 65 and 1 m a.s.l. (Figure 3(a), (c)). It shows a few transversal furrows and ridges and a very steep frontal scarp (> 40° in some points). The ST rock glacier is located at the foot of a talus and some debris flow cones and on its southern margin is adjacent to an ice-cored moraine of the Strandline Glacier (Figure 3(a), (c)).

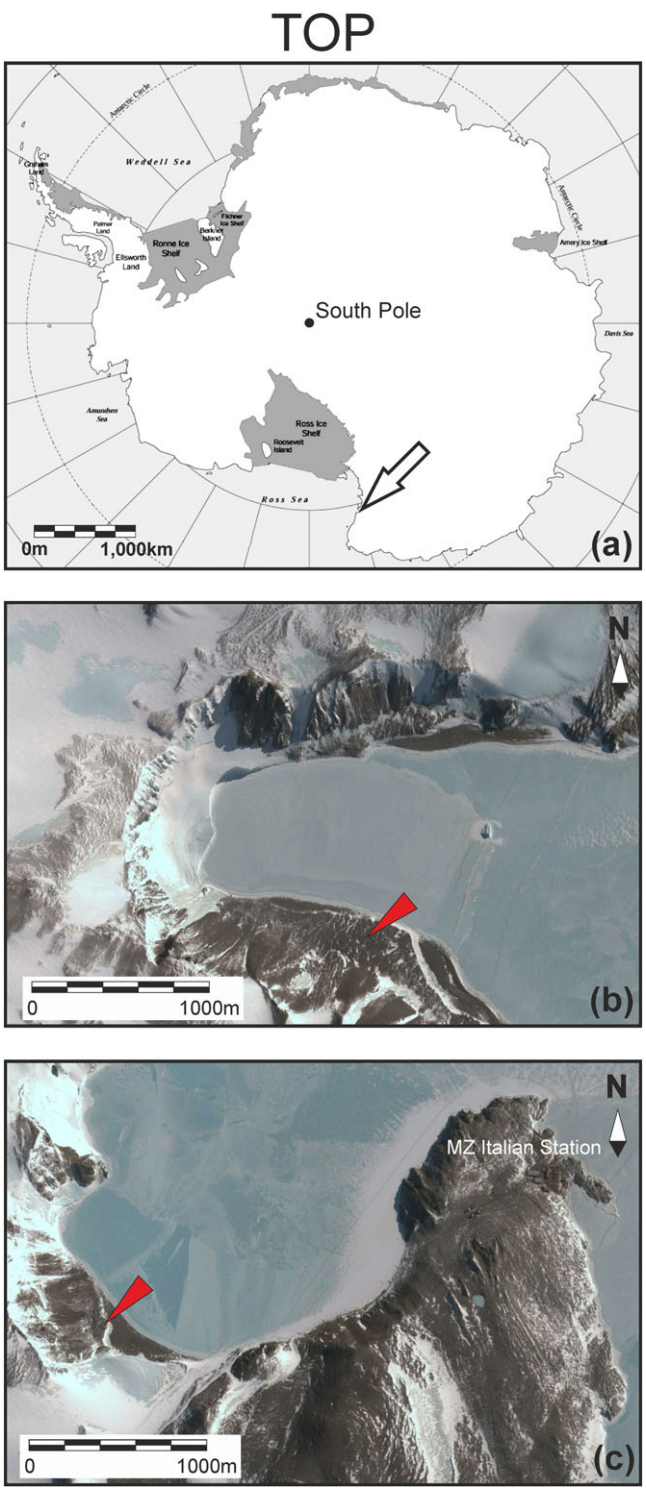

Figure 1. Location maps. (a) Map of Antarctica showing the location of the study area; (b) and (c) satellite photographs (courtesy Google Earth © DigitalGlobe 2016) of the Adélie Cove and Tethys Bay survey areas, respectively. [Colour figure can be viewed at wileyonlinelibrary.com]

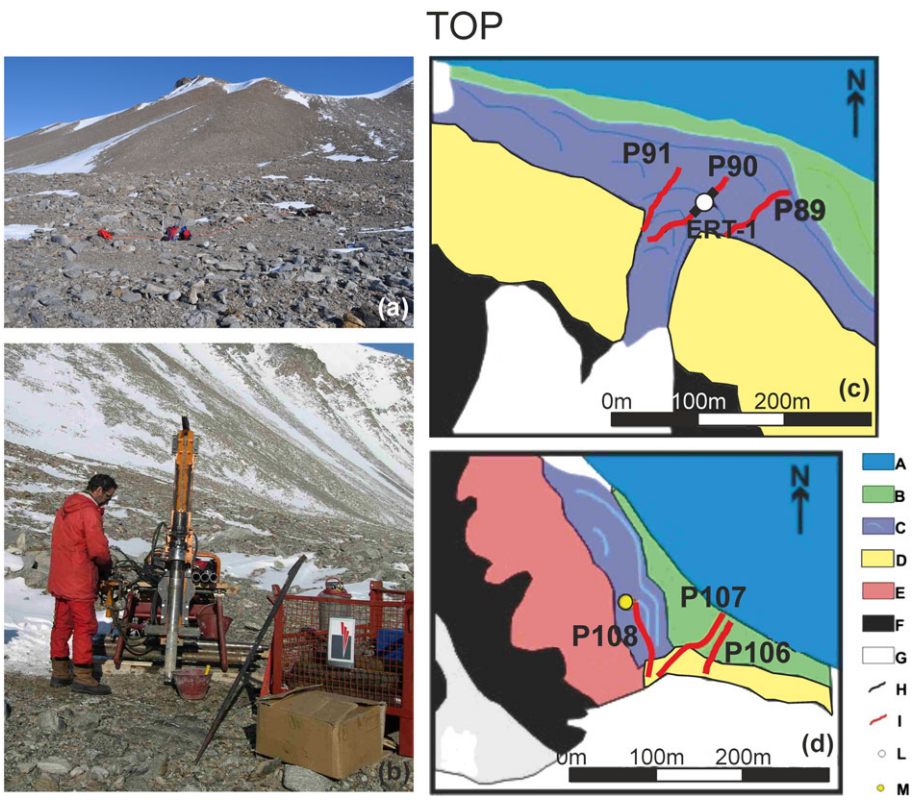

Figure 2. (a) Photograph of the ERT survey at Adélie Cove (11 November 2014); (b) photograph of the drilling operations at Adélie Cove (November 2003); (c) and (d) schematic geomorphological maps of the AD and ST areas, respectively, obtained by integrating the map of Baroni (1987) with analyses of aerial photographs and dedicated field surveys. Legend of the geomorphological maps: (A) sea; (B) beach deposits; (C) rock glaciers; (D) till and morainic ridges; (E) scree slopes with debris flows; (F) outcropping bedrock; (G) glaciers and snow banks; (H) ERT survey; (I) GPR profiles shown in the paper; (L) borehole; and (M) previously acquired Vertical Electric Soundings (VES). [Colour figure can be viewed at wileyonlinelibrary.com]

The AD rock glacier is a tongue-shaped rock glacier that is 510 m long and 280 m wide and is developed between 255 and 50 m a.s.l. (Figure 3(b), (d)). The rock glacier shows some transversal ridges and furrows and a very steep frontal scarp (>40°) that is very short because it overlaps another spatulate rock glacier (according to Baroni, 1987). The AD rock glacier

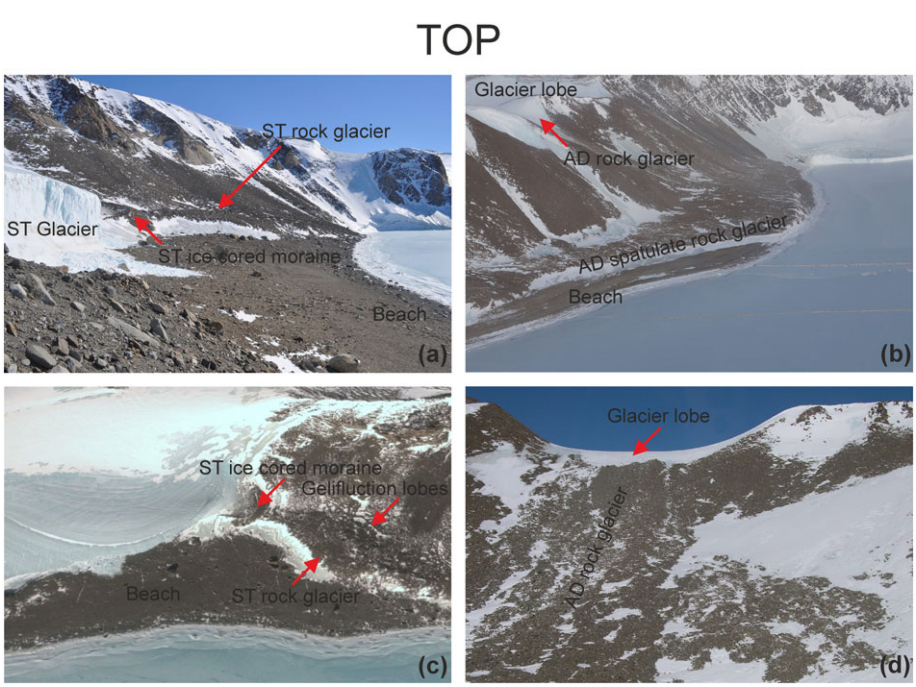

Figure 3. Views of the Adélie Cove and ST rock glaciers and their surroundings: (a) ST glacier, ice-cored moraine and rock glacier; (b) Adélie Cove South: from the sea to the upward margin, the raised beach, lower spatulate rock glacier and the AD rock glacier can be seen; (c) view from the central part of the ST rock glacier towards the ST glacier; and (d) AD rock glacier, with the glacier lobe clearly visible at its head. [Colour figure can be viewed at wileyonlinelibrary.com]

starts directly below a local glacier tongue without any visible discontinuities (Figure 3(b), (d)).

The AD and ST rock glaciers have already been studied. Indeed, Guglielmin *et al.* (1997), using DC vertical soundings, suggested that the ST rock glacier was very similar to an alpine ice-cemented rock glacier with a decreasing ice content with depth, whereas AD seemed to be an ice-cored rock glacier (probably glacier ice).

In contrast, French and Guglielmin (1999), on the basis of geomorphological data alone, suggested that the ST rock glacier might be a lateral moraine of the nearby Strandline Glacier partially overlapped by debris flows or snow avalanches coming from the upper slopes. The same authors also recalled that the deposit composing the ST was a till with several rounded cobbles of different lithological compositions but was not directly derived from the above granite back-wall.

Permafrost in the area is continuous and very thick, generally exceeding 400 m (Guglielmin, 2006). The active layer is very thin, ranging between 2 and 92 cm in the deposits (Guglielmin *et al.*, 2014), and it is strongly related to the surface conditions (generally thinner where mosses or lasting snow occur), although it can exceed 1.6 m in the granitic outcrops (Vieira *et al.*, 2010).

In this area, despite the stability of both mean annual air temperature (MAAT) and summer air temperature, the active layer thickness (ALT) is increasing at a rate up to 1 cm yr^{-1} (Guglielmin and Cannone, 2012), which is comparable with the higher rates recorded in the Arctic (Callaghan *et al.*, 2010; Christiansen *et al.*, 2010).

The climate of the area is characterized by a MAAT of –13.9°C (Frezzotti *et al.*, 2001). Precipitation, always in the form of snow, is very low and ranges between 100 and 200 mm yr^{-1} (Grigioni *et al.*, 1992; Monaghan *et al.*, 2006).

Methods

Field methods

Ground penetrating radar (GPR) and electrical resistivity tomography (ERT)

The objectives of the GPR surveys were to image the internal structures of the rock glaciers in the upper 10 m of sediments, whereas ERT was used to evaluate vertical and lateral variations mainly related to the different ice contents, typologies, and grain sizes. Indeed, the electrical resistivity is strongly increased when frozen materials are present, whereas it decreases by some orders of magnitude if there is some free water within the sediments. Moreover, materials with high resistivity, such as any frozen body, are characterized by low intrinsic attenuation and, therefore, electromagnetic (EM) waves can reach depths of several hundred metres or more (Plewes and Hubbard, 2001). All the surveys were undertaken on almost totally deglaciated areas (only metric snow patches were present, Figures 2(a) and 3).

For the GPR surveys, we used a ProEx GPR (Malå Geoscience) equipped with 250 MHz shielded antennas and triggered every 10 to 15 cm by an electro-mechanic odometer, and nine profiles with a total distance of approximately 1800 m were collected. ERT surveys were carried out with a 16G electro-resistivity metre (Pasi Geophysics) connected to 48 electrodes having constant separations of 2 m and adopting a standard Wenner electrode configuration.

A GPS was used for absolute GPR data positioning and dynamically recorded a position every 10 s. The achieved accuracies, with decimetric absolute errors in latitude/longitude and metric errors in elevation, were sufficient considering the type and objectives of the survey. The electrodes were positioned using the GPS in static mode, achieving an accuracy one order of magnitude higher.

Borehole investigations

To calibrate the geophysical investigation and to describe the stratigraphy of the rock glaciers, we used a 6.1 m long core extracted from a borehole drilled in the frontal part of AD (Figure 2(b)) using a widia bites core auger (Beretta T21) without any fluids in November 2003. The core was 101 mm in diameter, and the recovery rate was almost 100%, even though the recovered core was quite fractured. Due to logistical constraints, a second borehole on ST was not drilled.

The core samples were collected and delivered in a frozen state (–20°C) to Italy, where they were cut along their longitudinal diameters in a –20°C room. We present herein stratigraphic descriptions, gravimetric ice contents calculated according to Black (1965), ice type (based on bubble density and orientation) and electrical conductivities measured with an electrical conductivity meter (Hanna Instruments-HI 98360) with an accuracy of ±0.5%.

Moreover, some days after the drilling operations, temperature logging was carried out through a pt100 class A chain with an accuracy of ±0.1°C.

Data processing and analyses

The GPR data were processed using a standard processing flow that included drift removal (zero-time correction), background removal, geometrical spreading correction and exponential recovery, spectral analysis and bandpass filtering, topographic (static) correction and depth conversion. Stolt and Kirchhoff migrations were also tested and applied to the data. For depth conversion and migration, we estimated the electromagnetic velocity field using dedicated diffraction hyperbola analyses. The actual estimated velocity range was between 10 and 19 cm/ns; therefore, considering the errors and inaccuracies intrinsic to the method and the final objective of the survey, a constant value of 15 cm/ns was considered for spreading correction, depth conversion and migration, whereas for the data analysis, all the estimations were considered (Table I).

Table I. Synthesis of EM velocities resulting from the diffraction hyperbola analysis. The blue background marks AD, whereas the orange background marks the ST area

Profile n°	IP n°	Time [ns]	Velocity [cm/ns]
P89	1	40	16.5
P89	2	30	12.1
P89	3	57	16.1
P89	4	31	17.2
P90	1	40	13.3
P91	1	35	17.0
P91	2	49	19.2
P91	3	30	13.7
P106	1	35	13.0
P106	2	26	14.4
P106	3	27	10.8
P107	1	40	10.7
P107	2	56	9.5
P107	3	30	11.3
P108	1	54	15.8
P108	2	12	11.9
P108	3	6	17.8

To provide a more constrained GPR data interpretation, we analysed some 2D GPR attributes (Figures 3 and 7). This technique is currently routinely used for reflection seismic data (Chopra and Marfurt, 2007) but has not yet seen widespread application to GPR analysis. However, attributes were recently exploited in glaciological applications to obtain an improved characterization of the frozen materials in different environments (Colucci *et al.*, 2015; Forte *et al.*, 2016; Zhao *et al.*, 2016). Due to the intrinsic high resolution of GPR signals, attributes can emphasize vertical and lateral variations and aid in the definition of zones homogeneous for some physical parameters. In particular, we used phase- and frequency-related attributes, which can be useful to highlight the lateral continuity of reflectors and image domains with specific spectral characteristics, respectively, thus providing improved discrimination between zones with different attenuation properties.

The apparent resistivity data were inverted taking into account the topographic variations using the RES2DINV software program (Loke and Barker, 1996), which adopts a smoothness-constrained least-squares inversion algorithm to recover the true resistivity model. All the acquired data were edited before the inversion process to cancel out suspicious, noisy and out-of-range data. Due to the low temperatures during data acquisition and the presence of blocks on the surface in both surveys (Figure 2(a), (b)), the original data had quite low overall quality. We therefore removed 14% of the ERT-1 data.

The main factors that influence electrical resistivity in these landforms and that should be considered during data analyses for correct interpretations are (1) ice content, (2) temperature, especially considering the physical status changes occurring for water when the temperature is below zero °C and (3) salt content and possible related unfrozen water (e.g. brines). Grain size and mineralogical composition are generally less important because the constituting materials are normally unsorted in rock glaciers and ice-cored moraine deposits, with a prevalence of coarse materials (>sand) containing several different lithologies.

Results

AD rock glacier

AD geophysical investigations

On the AD rock glacier, there is a clear high-amplitude reflector, marked H0, that is mainly parallel to the surface

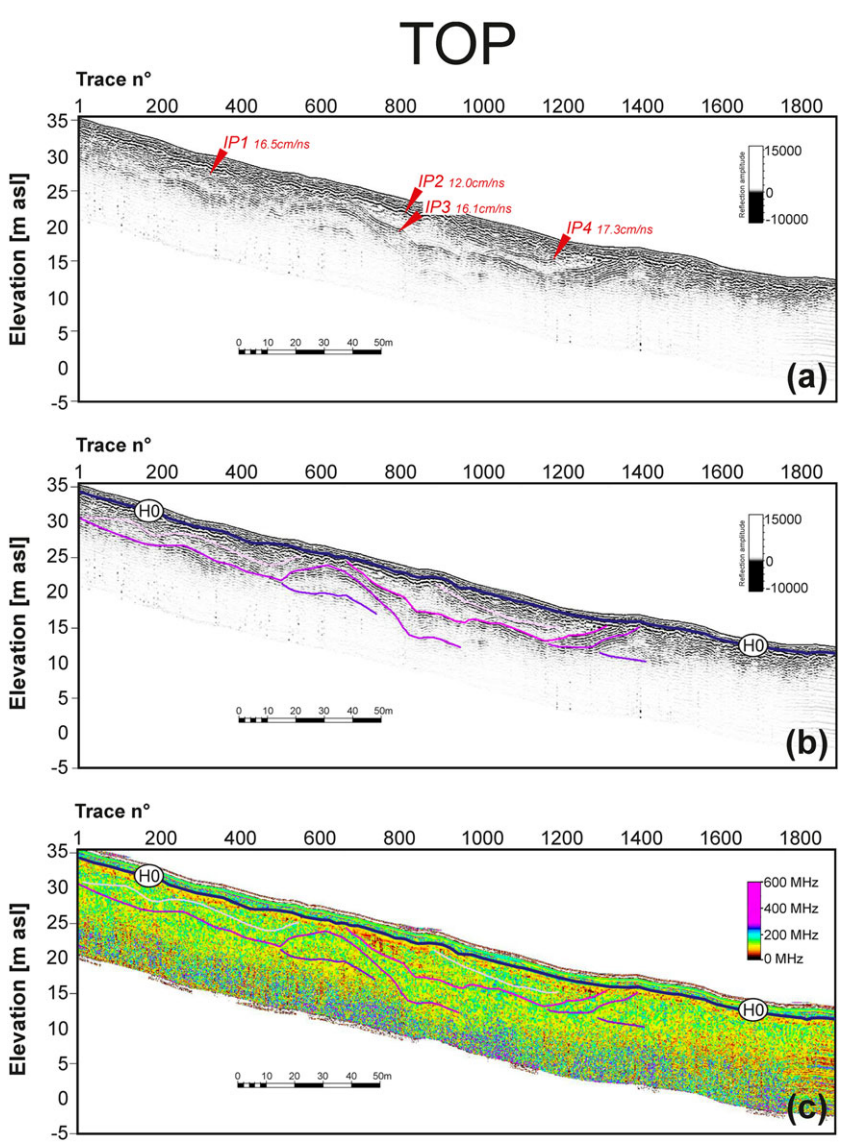

Figure 4. GPR profile P89 acquired at AD: (a) full-processed; (b) interpreted; and (c) instantaneous frequency interpreted. The blue line marks Horizon H0, whereas the purple lines are related to deeper levels. The red triangles point to the analysed hyperbolas, whose estimated velocities are reported in the labels. [Colour figure can be viewed at wileyonlinelibrary.com]

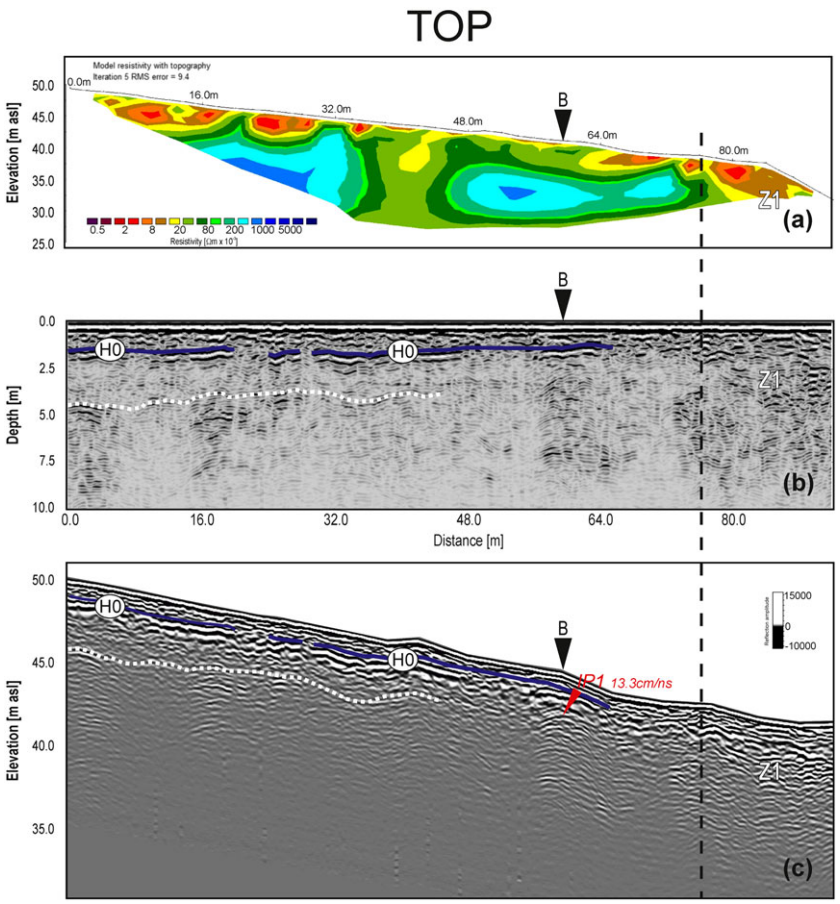

Figure 5. Comparison of the inverted ERT-1 section and the corresponding portion of the P90 GPR profile (Figure 2(c)), both of which were acquired in the AD area. Z1 highlights a zone characterized by relatively low resistivity and high electromagnetic scattering. Letter 'B' shows the location of the borehole, and the red triangle points to the analysed hyperbola, the estimated velocity of which is reported in the label. [Colour figure can be viewed at wileyonlinelibrary.com]

on all the GPR profiles (Figures 4, 5, and 6), although it is less continuous towards the sea. The reflector lies at a depth of approximately 1.2–1.6 m (Figure 4) and shows several high reflective layers with complex geometries (in purple) separated by electromagnetically low reflective or almost transparent bodies. The major parts of the reflectors are sub-parallel to the surface or slightly deformed and are not evidenced on the surface, with the exception of the counter slope reflector at approximately trace n° 1400 that is coincident with the front of a lobe within the rock glacier. Comparing the ERT and the corresponding portion of the GPR profile (Figure 5), there is rather good agreement. In fact, the shallowest part of the ERT section is always characterized by relatively low resistivity values (within the 3–20 kΩm range), whereas going to depths greater than 2–4 m, the resistivity values exceed 100 kΩm, with local maxima of approximately 1 MΩm.

Towards the coast (zone Z1), the resistivity tends to decrease (Figure 5(a)), but relatively low resistivity zones are also present in other portions of the study area. Within such zones, the horizon H0 imaged by the GPR survey is less continuous or even not recognized, whereas the attenuation of the electromagnetic signal is sensibly higher in compliance with the lower overall measured electrical DC resistivity.

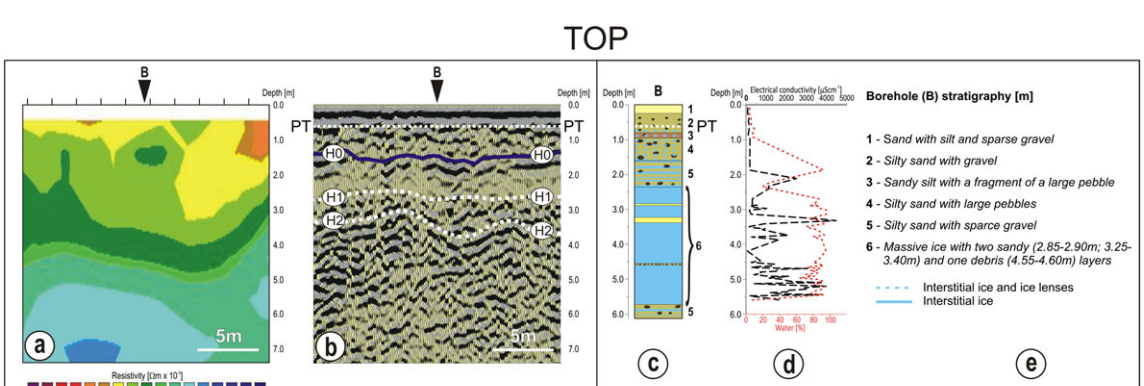

Figure 6. Borehole log and stratigraphy compared with a portion of GPR profile P90 and part of the ERT centred on the borehole in the Adélie Cove area. See the text for more details. [Colour figure can be viewed at wileyonlinelibrary.com]

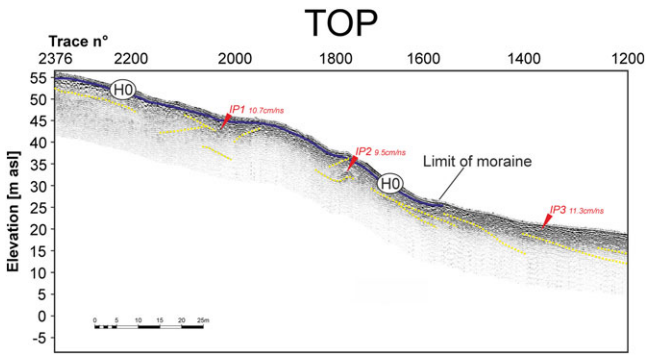

Figure 7. Part of the interpreted P107 (ST area) GPR profile. Horizon H0 is marked in blue, and deeper layers are highlighted by the yellow dotted lines. The red triangles point to the analysed hyperbolas, the estimated velocities of which are reported in the labels. [Colour figure can be viewed at wileyonlinelibrary.com]

AD borehole stratigraphy and temperature

From a lithological perspective, in the borehole log, we can recognize six different units (Figure 6) that from the top can be summarized as

1 0–0.25 m loose sand with silt and sparse max. 6 mm gravel grains,
2 0.25–0.8 m silty sand with gravel,
3 0.8–0.95 m sandy-silt with broken pebbles,
4 0.95–1.6 m silty sand with sub-rounded pebbles,
5 1.6–2.35 m and below 5.70 m silty sand with spare small pebbles and gravel.
6 2.35–5.70 m massive ice, including two sandy layers at depths of 2.85 and 3.25 m and a debris layer at 4.55 m.

From a cryological perspective, at the time of drilling (November 2003), the frost table (FT) was at 0.25 m, whereas the permafrost table (PT) was at 0.65 m. The first was identified as the minimum depth where some interstitial ice occurred, whereas PT was the depth where a sudden increase of ice content was detected. Neither has been imaged using geophysical data because they are too shallow. In fact, in GPR data, such layers were masked by ground wave arrivals, and PT is only speculatively detectable, whereas the ERT resolution was not sufficient to detect both of them using a minimum electrode spacing of 2 m. The ice content was generally low in the first 1.6 m of the core and was present only in the form of interstitial ice, whereas for depths between 1.6 and 2.35 m and below 5.7 m, it was highly variable with depth and was present as centimetric ice lenses and interstitial ice. A massive ice body (with an average ice content of approximately 85%) was detected at depths between 2.35 and 5.7 m. In the upper part (2.35–3.25 m), the ice was quite clean and lacked appreciable sediment layers, with the exception of a 5-cm-thick sandy layer (H1) at a depth of 2.85 m. Between 3.25 and 3.40 m, there was a thicker sand layer (H2), and below the ice, there were several millimetric silty-sandy layers and another 5 cm thick layer of debris at a depth of 4.55 m.

The first four lithological units in the core have quite low values of electrical conductivity (maximum 100 μS cm^{-1}) (Figure 6(d)), whereas unit 5 and in particular the massive ice body (unit 6) have values higher than 2500 μS cm^{-1} at depths of 2.12 and 3.32 m and in the lower part of the massive ice body.

As shown in Figure 6, the portion (20 m) of profile P90 centred on the borehole matched the stratigraphy fairly well. Indeed, the first possible reflector (PT) is located at an approximate depth of 0.6 m, where the permafrost table was identified in the borehole, whereas the strong reflector H0 corresponds to the first thick ice lens at an approximate depth of 1.6 m. The two deeper reflectors, H1 and H2, can be interpreted as the thicker sediment layers within the massive ice body at depths of approximately 2.85 and 3.30 m, respectively.

Although the borehole was drilled 10 years before the ERT and GPR surveys, it was undertaken during the same period of the year and therefore can be reasonably considered as a possible calibration for the geophysical investigations, obviously taking into account their resolution limits. The match between the stratigraphy and ERT seems less obvious; although the material above the PT has values lower than 12 kΩm, the portion between PT and H0 ranges between 12 kΩm and 30 kΩm, but below H0, the resistivity is definitely higher and increases with depth to more than 300 kΩm. Therefore, the general trend of increasing resistivity values with depth matches the increasing ice content, but the resolution is not sufficient to distinguish single stratigraphic or glaciological units.

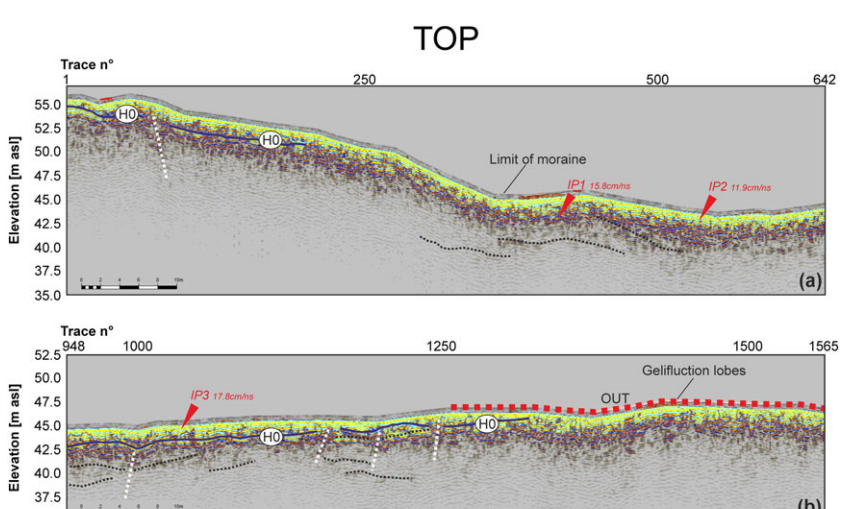

Figure 8. Two portions of the interpreted P108 GPR profile acquired in the ST area (from traces 1 to 642 and from traces 948 to 1565). Horizon H0 is marked in blue, and other deeper layers are highlighted by black dotted lines. The white dotted lines indicate possible crevasses, and the red line shows the zones with gelifluction lobes. The red triangles point to the analysed hyperbolas, the estimated velocities of which are reported in the labels. The 'OUT' label marks the zone where outcropping ice was observed during the field survey. [Colour figure can be viewed at wileyonlinelibrary.com]

ST rock glacier

A strong reflector that is mainly parallel to the surface (H0) also occurs at depths between 1.0 and 1.6 m on the ST rock glacier and adjacent ice-cored moraine, although it is sometimes discontinuous (Figure 7). Several deeper reflectors occur both in the ice-cored moraine and in the ST rock glacier (Figure 8), and from approximately trace n° 950 (Figure 8), several steep vertical structures resembling 'crevasses' interrupt H0 and the deeper reflectors. Moreover, there are fewer zones transparent to EM compared with AD, and a greater number of interfering events testify to the low homogeneity of the subsurface materials.

In the central part of the ST rock glacier, corresponding with some gelifluction lobes and some debris flows on the surface (Figure 8), the rock glacier presents a quite different structure that is characterized by a chaotic texture with minor discontinuous reflectors. This portion is characterized by the absence of transparent zones and appreciable clear, laterally continuous deeper reflectors.

Discussion

The GPR structures of both the AD and ST rock glaciers and the analysed ice-cored moraine highlight the widespread occurrence of a shallow reflector (always marked as H0) sub-parallel to the surface and roughly located between 1.0 and 1.6 m. At AD, the correlation of the reflector with the borehole stratigraphy (Figure 6) allows the reflector to be interpreted as the beginning of a cryo-lithological unit that is characterized by thick ice lenses responsible for low electrical conductivity. Below H0, almost everywhere more discontinuous reflectors from sub-parallel to the surface to counter slopes occur. These reflectors correspond in the borehole to sediment layers within massive ice, and in some cases, their counter slopes seem to be related to the surface topography because they correspond to frontal scarps or ridges within the rock glacier body (e.g. Figure 4 around trace 1400).

The sediment layers herein described resemble the Inclined Debris Layers (IDL) found in the Mullins and Friedman debris-covered glaciers in the Dry Valleys (Mackay and Marchant, 2017). Using GPR data, those authors also detected sediment layers that slope upward in correspondence with arcuate topographic ridges on the surface that are interpreted as being related to climate changes in the Pleistocene.

The massive ice occurring in the AD borehole between depths of 2.35 and 5.7 m is generally bubbly, with spherical bubbles that are randomly distributed but never elongated (Figure 9). The densities of the bubbles are normally low, but some centimetric layers have higher densities (more specifically, at 2.35, 2.55, 2.75, 2.85, 3.05, 3.60, 3.80, 3.88, 4.00, 4.38, 4.45, and 4.50 m). On the other hand, the bubbles are generally iso-oriented and organized in fine bands with

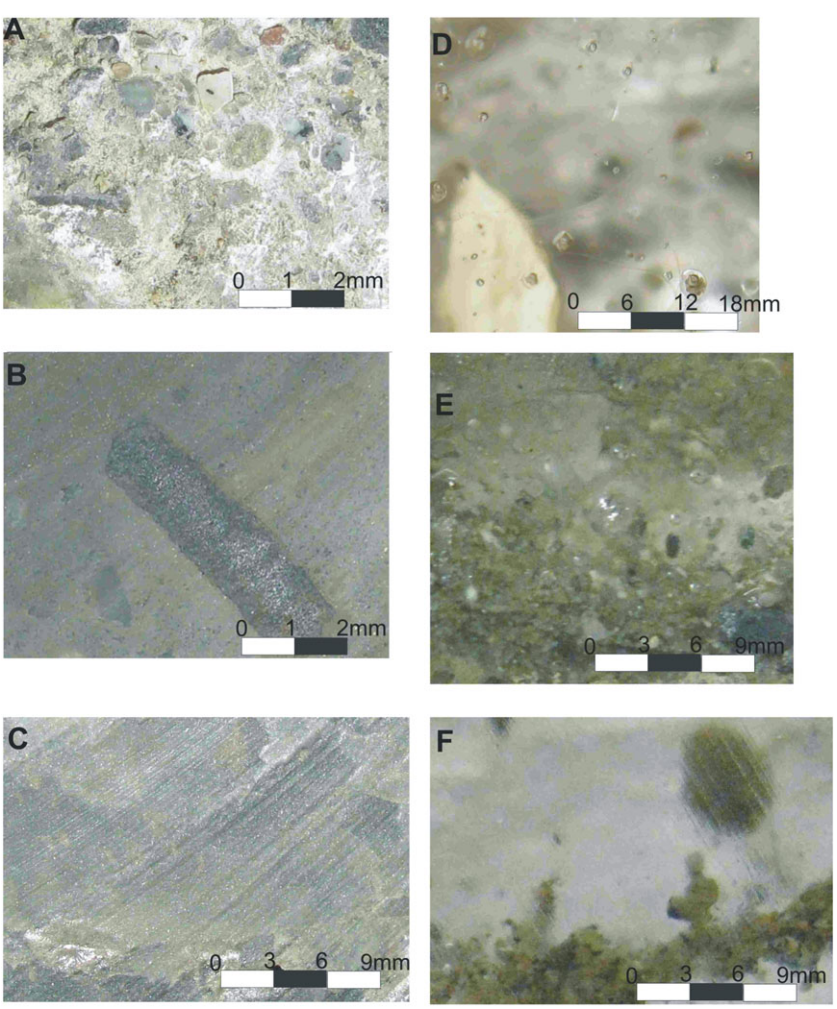

Figure 9. Details of the AD core and ice characteristics at different depths: (a) 20–40 cm, where the low content of interstitial ice is visible (whitish areas); (b) 95–100 cm (almost no interstitial ice is visible); (c) 160–165 cm, where ice lenses alternated to sand can be seen; (d) 290–295 cm, showing almost clear ice with some spherical bubbles; (e) 445–450 cm, showing dirty ice with randomly distributed spherical bubbles; and (f) at 545–550 cm, where a thin debris layer within almost pure clear ice is visible. [Colour figure can be viewed at wileyonlinelibrary.com]

different dips that can be vertical (at a depth of 2.95 m). In addition, the electrical conductivity (Figure 6(d)), especially in the lower part of the massive ice, shows alternating high and low values that are difficult to relate to the freezing of ground water but that are very similar to what occurs in cold glacier ice. According to some authors (Haeberli *et al.*, 2006), the meaning of 'glacier ice' is not clear, both because glaciers receive their ice from a variety of different sources and processes and because the ice changes through time due to glacial deformation in a similar way as in rock glaciers (flow metamorphism) (Berthling, 2011). In contrast, although the physical characteristics of massive ice cores such as the core that we found at AD are not definitive for the attribution of ice genesis, if we consider the massive ice core in its climatological and geological context, it is reasonable that this massive ice body should be a remnant of glacier ice. Indeed, the combined effects of generally very low snow precipitation, high sublimation rates and strong winds typical of a large part of the continental Antarctica strongly reduce the possibility of the permanent snow banks that are so common in alpine permafrost areas and are, in turn, considered the main source of massive ice bodies within rock glaciers (Haeberli *et al.*, 2006). Furthermore, the occurrence of a glacier lobe just upward of AD without any apparent discontinuity and fed from behind by a large glacier excludes one of the arguments reported by Haeberli and Vonder Mühll (1996) and Haeberli (2000), in which the term 'glacier-derived' is rejected because, as they stated, ice bodies at the heads of 'glacier-derived' rock glaciers are smaller than true glaciers.

If we extend the borehole calibration at AD to the rock glacier and ice-cored moraine at ST, we can reasonably state that they are both characterized by a massive glacier ice body with several stratifications (IDLs) detectable by GPR, even if in the ST area the ice is probably 'dirtier' because it is less transparent from the EM perspective and there are many interfering diffractions that are possibly due to sediments and blocks.

In addition, the sub-vertical structures resembling 'crevasses' occurring at ST in both the rock glaciers and the ice-cored moraine confirm some observations already proposed by French and Guglielmin (1999) for other presumed periglacial landforms such as gelifluction terraces, where steps 'might reflect small faults or crevasses in the ice caused by irregularities in the underlying bedrock'.

The absence of 'crevasses' and stratifications within the massive glacier ice in the central part of the ST rock glacier (at least until the depth of penetration of the GPR) may be due to the interaction between the relict glacier ice and debris flows and gelifluction lobes coming from the above scree slope that just overlie the massive glacier ice.

Moreover, additional information on the internal structure of the analysed landforms can be obtained using EM velocities. First, it is important to note that in all the surveyed areas the number of isolated scatterers producing clear diffraction hyperbolas is limited, preventing a detailed reconstruction of the EM velocity field such as that recently reported for South American rock glaciers by Monnier and Kinnard (2013 and 2015). In any case, we remark that even in such favourable conditions, the exclusive use of diffraction hyperbola analyses is intrinsically imprecise due to the presence of combined reflection and diffraction events or interfering phenomena at different scales more generally. Therefore, only multifold techniques (Forte and Pipan, 2017) or specific inversion strategies (Forte *et al.*, 2014) can provide accurate velocity field estimations. Diffractions occur when a transmitted GPR wave reaches 'objects' with dimensions roughly equal to the mean EM wavelength (Jol, 2009). By considering that the central frequency of the utilized antennas is equal to 250 MHz and that, as already reported, the mean EM velocity is approximately 15 cm/ns, we can argue that we should have an approximately 0.75-m-wide target to produce pure diffraction (Kirchhoff criterion). We can therefore argue that targets of such dimensions are only seldom present in both surveyed areas, at least within the depths imaged by the GPR. We remark that due to the extremely rough topography, either single Common Mid Point (CMP) measurements or multifold profiles aimed at a more precise and constrained velocity field estimation would be virtually impossible to acquire.

In the AD rock glacier, the EM velocities vary between 12.1 and 19.2 cm/ns and have an average of 15.6 cm/ns (Table I), but if we consider only the velocities calculated on hyperbolas deeper than 2 m, they range between 16.1 and 19.2 cm/ns, which are values typical of frozen materials (Forte *et al.*, 2013). Hyperbola IP1 on profile P90 (Figure 5(c)) is particularly significant because the estimated value of 13.3 cm/ns is referred to *c.* 0.6 m of unfrozen sediments overlying *c.* 2 m of frozen sediments with less than 30% interstitial and segregated ice (except for the H0 reflector, where the ice content exceeds 85% (see Figure 6(d))), indicating that a relatively small amount of ice does not strongly influence EM velocity. In contrast, hyperbola IP3 on profile P108 (Figure 8), with a value of 17.8 cm/ns, is representative of massive ice, which at that point is almost outcropping. Unfortunately, at ST, we did not find appreciable hyperbolas in the ice-cored moraine or in the central part characterized by gelifluction lobes and debris flow ridges. However, there are some elements that suggest the presence of massive ice also in the ST area, namely: (1) EM velocity values exceeding 15 cm/ns very close to the topographic surface (IP3 on Figure 8(b); (2) local ice outcrops ('OUT' on Figure 8(b)); and (3) crevasse-like structures (Figure 8(a), (b)). The occurrence of pure ice so close to the ST rock glacier surface could corroborate the original interpretation of the ST rock glacier as a lateral ice-cored moraine (French and Guglielmin, 1999) partially overlapped by gelifluction lobes and debris flow ridges in its central part that simulate typical rock glacier flow structures.

The Vertical Electric Sounding (VES A4) reported in Guglielmin *et al.* (1997) and centred in this area revealed electrical resistivities lower than 20 kΩm between depths of 1.1 and 3.9 m and more than 100 kΩm between depths of 3.9 and 20 m; those reported resistivities were always lower than the ones we found corresponding to the massive ice calibrated at the AD borehole, where the electrical resistivity was more than 300 kΩm. Ascribing causes for these lower electrical resistivity values in the central part of the ST rock glacier is difficult, but it is probably that the less EM transparent ice of the ST rock glacier and its lateral continuity with the ice-cored moraine of the Strandline glacier could suggest higher debris contents in the buried ice of the ST rock glacier that further increase below the debris flows and gelifluction lobes areas.

The use of combined GPR and ERT is surely a valid tool to understand the internal structures of landforms such as rock glaciers, debris-covered glaciers and ice-cored moraines, especially in the cryotic environment of the polar areas (Moorman *et al.*, 2003; De Pascale *et al.*, 2008). Our data confirm that the combination of the two geophysical methods gives more valuable results, but it is essential to properly calibrate both because electrical resistivity and dielectric permittivity are controlled by several interacting parameters that are difficult to distinguish and separate.

Considering the thermal log in the AD borehole (Figure 10, red line), we can see that the temperature decreased from –12.2°C at 0.6 m to –15.2°C at 3.75 m. At those low values of

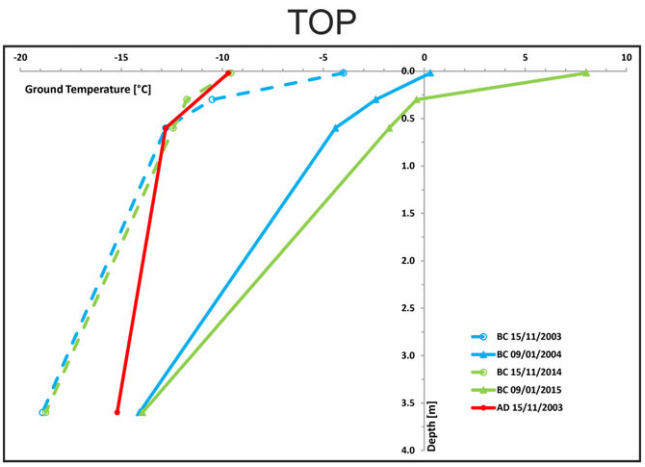

Figure 10. Temperature logs performed in the AD borehole (red line) and in a borehole at Boulder Clay (BC). See the text for details. [Colour figure can be viewed at wileyonlinelibrary.com]

temperature, although the measured electrical conductivity was relatively high on average (probably indicating a high salt content), the unfrozen water can be considered negligible, if any, and below 3.25 m, the electrical resistivity was therefore quite high due to the high ice content. Figure 10 shows for comparison some temperature logs of a borehole monitored since 1996 at Boulder Clay (BC), approximately 2 km north of AD (Guglielmin and Cannone, 2012; Guglielmin *et al.*, 2014). Because we were unable to measure the log temperature at AD in 2014 during the geophysical surveys, we compared previous data at AD (November 2003, red line) with temperature data during the same period at BC (dashed light blue line). We observe that the two logs were similar in the upper parts (above depths of 60 cm), whereas AD was sensibly warmer at greater depths. Moreover, although the November temperatures at BC did not change significantly between 2003 and 2014 during maximum warming, it is possible to see that the temperature close to the permafrost table at BC increased in the same period from –2.5°C to –0.5°C. This behaviour confirms that the thickness of the active layer has increased by approximately 0.7 cm/y in the last 20 years (Guglielmin *et al.*, 2014). If this kind of warming continues in the coming years, it is apparent that where massive buried glacier ice occurs in the first decimetres, as we found in some parts of the ST rock glacier or in the ice-cored moraine at Tethys Bay, thermokarst features could start to develop. This phenomenon is particularly important for human infrastructure, including the proposed airstrip construction at Boulder Clay and related planned service roads.

It is interesting to highlight that the geophysical surveys and the GPR data in particular show the occurrence of ice lenses and massive ice with high accuracies in terms of location and persistence. The tops of these ice-rich zones are imaged by a high reflective horizon (H0) sub-parallel to the topographic surface. That geometry could wrongly suggest interpreting that reflector as the base of the active layer, but as demonstrated by the borehole stratigraphy and logs at AD (Figure 6), it rather represents an abrupt increase in ice content in a cryo-lithological unit characterized by several ice lenses within the sediments. H0 therefore marks the increasing ice content from interstitial to more massive ice. Some authors have pointed to the presence of a 'transition zone' (TZ) or 'transient layer' between the active layer and the permafrost (Shur *et al.*, 2005). The base of the TZ represents the long-term permafrost table and is important for permafrost stability because it acts as a sort of buffer between the active layer and ice-rich permafrost, especially for permafrost containing massive ice (Shur *et al.*, 2005). This zone can enlarge and change properties over time through ice segregation, the infiltration of meteoric water or melting ground ice from the overlying active layer (Hinkel and Nelson, 2003). The subsequent segregation and refreezing produce ice lenses, which are more common and developed at increasing depths because the uppermost part of the TZ undergoes thawing more frequently. From a geophysical perspective, as far as we know, such a TZ has never been clearly interpreted, even though it was somehow recognized and imaged by Monnier and Kinnard (2015), and it is often generically and simplistically interpreted as the base of the active layer.

The TZ has a crucial impact on the processes that gradually transform the upper permafrost, the formation of cryogenic structures and the thermal stability of permafrost in the face of climatic variations, but despite the importance of this layer, it still has been considered in only a few works (Shur *et al.*, 2005).

Conclusions

This paper has demonstrated that two rock glaciers located in the Northern Victoria Land (AD and ST) mapped originally as Holocene periglacial landforms by Baroni (1987) and afterwards considered to be ice-cored rock and ice-cemented rock glaciers, respectively, based only on VES results (Guglielmin *et al.*, 1997) are now both interpreted to have glacial origins as a result of integrated geophysical investigations (GPR and ERT) and borehole stratigraphy. In fact, we highlight that both glaciers have similar internal structures, including cores of buried glacier ice. As a consequence, these landforms are most likely due to the creep of the buried ice occurring in the landforms rather than to permafrost creep.

From a geophysical perspective, we have shown that sediments containing ice and 'dirty' ice can exhibit similar electrical resistivity values spanning a quite wide range from some tens of kΩm up to some MΩm, so that interpretation is not straightforward in the absence of auxiliary data. In the GPR data, the ice sometimes is imaged as EM transparent facies with high velocities typical of frozen water, whereas in other cases, the ice is characterized by a chaotic texture with several interfering events testifying to the low homogeneity of the subsurface materials. The first facies is typical of cold glacial ice with minor alternating sediments (Figure 4), as recently discussed by McCarthy *et al.* (2017) and by Mackay and Marchant (2017) for debris-covered glaciers in Nepal and Antarctica, respectively. In the case of a more chaotic texture, we inferred the presence of 'dirtier' ice or of intercalations of ice and sediments, with local rocky blocks and possible crevasses (Figure 8).

The results of this paper probably can be extended to the large majority of Antarctic rock glaciers or at least to the rock glaciers in Continental Antarctica because, to our knowledge, all the boreholes and shallow excavations in Antarctica (Fukui *et al.*, 2008; Swanger *et al.* 2010; Vieira *et al.*, 2012; Bockheim, 2014) have found massive ice at very shallow depths, as in our case, and because their morphological locations and their relationships with the surrounding glaciers are similar to those found in our two study cases.

From a methodological perspective, combining all the available data, we conclude that the rather continuous, high-reflective GPR horizon sub-parallel to the topographic surface cannot be interpreted as the base of the active layer but rather represents the top of a cryo-lithological unit characterized by ice lenses within the sediments. That unit is related to the TZ between the active layer and the permafrost,

which is the long-term permafrost table at the base of the TZ. Although the TZ has not yet been fully explored, it is surely important to permafrost stability because it acts as a sort of buffer between the active layer and ice-rich permafrost, especially in areas where the permafrost contains massive ice.

More generally, knowledge of subsurface ice content and in particular the occurrence of massive ice and its depth is crucial in the more developed cryotic areas in the Northern and Southern hemispheres in order to make realistic and affordable forecasts of thermokarst development and related feedback GHG emissions, especially in the case of cryosoils rich in carbon content.

Further research could be undertaken that combines GPR and Induced Polarization techniques, which could increase overall resolution and reduce survey times in comparison with those of ERT surveys.

Acknowledgements—This project was funded by Italian PNRA grant 2013/AZ1.05, 'Permafrost ecology in Victoria Land'; we would like to thank all the people from PNRA who provided the logistical support needed to carry out the research. We further thank Maurizio Azzaro and Michele Dalle Fratte for their help during field operations. We gratefully thank Halliburton and Schlumberger, who provided support through the University of Trieste ProMAX® (processing suite) and Petrel® (interpretation package) academic grants. We would also like to thank Fabio Baio and Andrea Strini, who drilled the AD borehole, and Roberto Gambillara, Marco Filippazzi and Andrea Strini for the laboratory analyses.

Both the authors wrote the paper and together with Maurizio Azzaro and Michele Dalle Fratte undertook the geophysical fieldwork. The laboratory analyses were undertaken by Stefano Ponti, who also contributed to the preparation of the paper.

References

Arenson LU, Hoelzle M, Springman S. 2002. Borehole deformation measurements and internal structure of some rock glaciers in Switzerland. *Permafrost and Periglacial Processes* **13**: 117–135.

Azócar GF, Brenning A. 2010. Hydrological and geomorphological significance of rock glaciers in the dry Andes, Chile (27°–33°S). *Permafrost and Periglacial Processes* **21**: 42–53.

Baroni C. 1987. Geomorphological map of the Northern Foothills near the Italian station. *Memorie della Societa Geologica Italiana* **33**: 195–211.

Baroni C, Orombelli G. 1987. Glacial geology and geomorphology of Terra Nova Bay (Victoria Land, Antarctica). *Memorie della Societa Geologica Italiana* **33**: 171–193.

Berthling I. 2011. Beyond confusion: rock glaciers as cryo-conditioned landforms. *Geomorphology* **131**: 98–106.

Berthling I, Etzelmüller B, Isaksen K, Sollid JL. 2000. The rock glaciers on Prins Karls Forland Svalbard (II). GPR soundings and the development of internal structures. *Permafrost and Periglacial Processes* **11**: 357–369.

Black CA. 1965. *Methods of Soil Analysis: Part I. Physical and Mineralogical Properties*. American Society of Agronomy: Madison, Wisconsin, USA.

Bockheim JG. 2014. Distribution properties and origin of viscous-flow features in the McMurdo Dry Valleys Antarctica. *Geomorphology* **204**: 114–122.

Callaghan TV, Bergholm F, Christensen TR, Jonasson C, Kokfelt U, Johansson M. 2010. A new climate era in the subArctic: accelerating climate changes and multiple impacts. *Geophysical Research Letters* **37**: L14705.

Capps SR, Jr. 1910. Rock glaciers in Alaska. *Journal of Geology* **18**: 359–375.

Chopra S, Marfurt KJ. 2007. *Seismic attributes for prospect identification and reservoir characterization*, SEG geophysical developments series no. 11. Society of Exploration Geophysicists: Tulsa, OK, USA.

Christiansen HH, Etzelmüller B, Isaksen K, Juliussen H, Farbrot H, Humlum O, Johansson M, Ingeman-Nielsen T, Kristensen L, Hjort J, Holmlund P, Sannel ABK, Sigsgaard C, Åkerman HJ, Foged N, Blikra LH, Pernosky MA, Ødegård RS. 2010. The thermal state of permafrost in the nordic area during the international polar year 2007–2009. *Permafrost and Periglacial Processes* **21**: 156–181.

Clark DH, Steig EJ, Potter NJ, Fitzpatrick J, Updike AB, Clark GM. 1996. Old ice in rock glaciers may provide long term climate records. *EOS. Transactions of the American Geophysical Union* **77**: 217–222.

Colucci RR, Boccali C, Zebre M, Guglielmin M. 2016. Rock glaciers, protalus ramparts and pronival ramparts in the south-eastern Alps. *Geomorphology* **269**: 112–121.

Colucci RR, Forte E, Boccali C, Dossi M, Lanza L, Pipan M, Guglielmin M. 2015. Evaluation of internal structure volume and mass balance of glacial bodies by integrated LiDAR and GPR surveys: the case study of Canin Eastern Glacieret (Julian Alps Italy). *Surveys in Geophysics* **36**: 231–252.

De Pascale GP, Pollard WH, Williams KK. 2008. Geophysical mapping of ground ice using a combination of capacitive coupled resistivity and ground-penetrating radar Northwest Territories Canada. *Journal of Geophysical Research* **113**: F02S90.

Degenhardt JJ, Jr. 2009. Development of tongue-shaped and multilobate rock glaciers in alpine environments – interpretations from ground penetrating radar surveys. *Geomorphology* **109**: 94–107.

Degenhardt JJ, Giardino JR, Junck MB. 2003. GPR survey of a lobate rock glacier in Yankee Boy Basin Colorado USA. In *Ground Penetrating Radar in Sediments*, Bristow CS, Jol HM (eds), Vol. **211**. Special Publication: Geological Society of London; 167–179.

Doran PT, Priscu JC, Lyons WB, Walsh JE, Fountain AG, McKnight DM, Moorhead DL, Virginia RA, Wall DH, Clow GD, Fritsen CH, McKay CP, Parsons AN. 2002. Antarctic climate cooling and terrestrial ecosystem response. *Nature* **415**: 517–520.

Evin M, Fabre D. 1990. The distribution of permafrost in rock glaciers of Southern Alps (France). *Geomorphology* **3**: 57–71.

Forte E, Pipan M. 2017. Review of multi offset GPR applications: data acquisition processing and analysis. *Signal Processing* **132C**: 210–220.

Forte E, Dossi M, Colucci RR, Pipan M. 2013. A new fast methodology to estimate the density of frozen materials by means of common offset GPR data. *Journal of Applied Geophysics* **99**: 135–145.

Forte E, Dossi M, Pipan M, Colucci RR. 2014. Velocity analysis from Common Offset GPR data inversion: theory and application to synthetic and real data. *Geophysical Journal International* **197**: 1471–1483.

Forte E, Dalle Fratte M, Azzaro M, Guglielmin M. 2016. Pressurized brines in Continental Antarctica as possible analog of Mars. *Scientific Reports* **6**: 33158 https://doi.org/10.1038/srep33158.

Fountain AG, Levy JS, Gooseff MN, Van Horn D. 2014. The McMurdo Dry Valleys: a landscape on the threshold of change. *Geomorphology* **225**: 25–35.

French HM, Guglielmin M. 1999. Observations on the ice marginal periglacial geomorphology of Terra Nova Bay Northern Victoria Land Antarctica. *Permafrost and Periglacial Processes* **10**: 331–348.

Frezzotti M, Salvatore MC, Vittuari L, Grigioni P, De Silvestri L. 2001. Satellite image map: northern foothills and inexpressible island area (Victoria Land Antarctica). *Terra Antarctica Reports* **6**: 1–8 plus map.

Fukui K, Sone T, Strelin J, Torielli C, Mori J. 2007. Ground penetrating radar sounding on an active rock glacier on James Ross Island Antarctic Peninsula region. *Polish Polar Research* **28**: 13–22.

Fukui K, Sone T, Strelin JA, Torielli CA, Mori J, Fujii Y. 2008. Dynamics and GPR stratigraphy of a polar rock glacier on James Ross Island, Antarctic Peninsula. *Journal of Glaciology* **54**: 445–451.

Grigioni P, De Silvestri L, Pellegrini A, Sarao L. 1992. Some climatological aspects in the Terra Nova Bay Area Antarctica. In *Italian Research on Antarctic Atmosphere*, Colacino M, Giovanelli G, Stefanutti L (eds). CNR: Bologna; 97–121.

Guglielmin M. 2004. Observations on permafrost ground thermal regimes from Antarctica and the Italian Alps and their relevance to global climate change. *Global and Planetary Change* **40**: 159–167.

Guglielmin M. 2006. Ground surface temperature (GST) active layer and permafrost monitoring in continental Antarctica. *Permafrost and Periglacial Processes* **17**: 133–143.

Guglielmin M, Cannone N. 2012. A permafrost warming in a cooling Antarctica? *Climatic Change* **111**: 177–195.

Guglielmin M, Lozej A, Tellini C. 1994. Permafrost distribution and rock glaciers in the Livigno Area (Northern Italy). *Permafrost and Periglacial Processes* **5**: 1–12.

Guglielmin M, Biasini A, Smiraglia C. 1997. Buried ice landforms in the Northern Foothills (Northern Victoria Land Antarctica). Some results from electrical soundings. *Geographiska Annaler* **79a**: 17–24.

Guglielmin M, Cannone N, Dramis F. 2001. Permafrost-glacial evolution during the Holocene in the Italian Central Alps. *Permafrost and Periglacial Processes* **12**: 111–124.

Guglielmin M, Lewkowicz A, French HM, Strini A. 2009. Lake-ice blisters Terra Nova Bay area Northern Victoria Land Antarctica. *Geografiska Annaler A* **91**: 99–111.

Guglielmin M, Dalle Fratte M, Cannone N. 2014. Permafrost warming and vegetation changes in continental Antarctica. *Environmental Research Letters* **9**: 045001.

Haeberli W. 1985. Creep of mountain permafrost. *Mitteilungen der Versuchsanstalt für Wasserbau Hydrologie und Glaziologie der ETH Zürich* **77**: 142.

Haeberli W. 2000. Modern research perspectives relating to permafrost creep and rock glaciers: a discussion. *Permafrost and Periglacial Processes* **11**: 290–293.

Haeberli W, Vonder Mühll D. 1996. On the characteristics and possible origin of ice in rock glacier permafrost. *Zeitschrift für Geomorphologie* **104**(Suppl. Bd): 43–57.

Haeberli W, Hallet B, Arenson L, Elconin R, Humlum O, Kääb A, Kaufmann V, Ladanyi B, Matsuoka N, Springman S. 2006. Permafrost creep and rock glacier dynamics. *Permafrost and Periglacial Processes* **17**: 189–214.

Hartl L, Fischer A, Klug C, Nicholson L. 2016. Can a simple numerical model help to fine-tune the analysis of ground-penetrating radar data? Hochebenkar Rock Glacier as a case study. *Arctic Antarctic and Alpine Research* **48**: 377–393.

Hassinger JM, Mayewski PA. 1983. Morphology and dynamics of the Rock Glaciers in Southern Victoria Land Antarctica. *Arctic and Alpine Research* **15**: 353–368.

Hauck C. 2001. Geophysical methods for detecting permafrost in high mountains. *Versuchsanstalt für Wasserbau Hydrologie und Glaziologie ETH Mitteilungen* **171**: 204.

Hauck C, Guglielmin M, Isaksen K, Vonder MD. 2001. Applicability of frequency-domain and time-domain electromagnetic methods for mountain permafrost studies. *Permafrost and Periglacial Processes* **12**: 39–52.

Hausmann H, Krainer K, Brückl E, Mostler W. 2007. Internal structure and ice content of Reichenkar rock glacier (Stubai Alps Austria) assessed by geophysical investigations. *Permafrost and Periglacial Processes* **18**: 351–367.

Hinkel KM, Nelson FE. 2003. Spatial and temporal patterns of active layer thickness at circumpolar active layer monitoring (CALM) sites in northern Alaska 1995–2000. *Journal of Geophysical Research* **108**: 8168–8168.

Humlum O. 1998. The climatic significance of rock glaciers. *Permafrost and Periglacial Processes* **9**: 375–395.

IPCC. 2013. Summary for Policymakers. In *Climate Change 2013: The Physical Science Basis*, Stocker TF, Qin D, Plattner GK, Tignor M, Allen SK, Boschung J, Nauels A, Xia Y, Bex V, Midgley PM (eds), Contribution of Working Group I to the Fifth Assessment Report of the Intergovernmental Panel on Climate Change. Cambridge University Press: Cambridge, UK and New York, USA.

Janke JR, Bellisario AC, Ferrando FA. 2015. Classification of debris-covered glaciers and rock glaciers in the Andes of central Chile. *Geomorphology* **241**: 98–121.

Jol HM (ed). 2009. *Ground Penetrating Radar: Theory and Applications*. Elsevier Science: The Netherlands.

Kellerer-Pirklbauer A, Lieb GK, Kleinferchner H. 2012. A new rock glacier inventory of the eastern European Alps. *Austrian Journal of Earth Sciences* **105**: 78–93.

King L, Fisch W, Haeberli W, Wächter HP. 1987. Comparison on resistivity and radio-echo soundings on rock glacier permafrost. *Zeitschrift für Gletscherkunde und Glazialgeologie* **23**: 77–97.

Krainer K, Bressan D, Dietre B, Haas NJ, Hajdas I, Lang K, Mair V, Nickus U, Reidl D, Thies H, Tonidandel D. 2015. A 10300-year-old permafrost core from the active rock glacier Lazaun southern Ötztal Alps (South Tyrol northern Italy). *Quaternary Research* **83**: 324–335.

Lehmann F, Green A. 2000. Topographic migration of georadar data: implications for acquisition and processing. *Geophysics* **65**: 836–848.

Leopold M, Williams MW, Caine N, Völkel J, Dethier D. 2011. Internal structure of the Green Lake 5 rock glacier Colorado Front Range USA. *Permafrost and Periglacial Processes* **22**: 107–119.

Lilleøren KS, Etzelmüller B. 2011. A regional inventory of rock glaciers and ice-cored moraines in Norway. *Geografiska Annaler A* **93**: 175–191.

Loke MH, Barker RD. 1996. Rapid least-squares inversion of apparent resistivity pseudosections by quasi-Newton method. *Geophysical Prospecting* **44**: 131–152.

López-Martínez J, Serrano E, Schmid T, Mink S, Linés C. 2012. Periglacial processes and landforms in the South Shetland Islands (northern Antarctic Peninsula region). *Geomorphology* **155–156**: 62–86.

Mackay SL, Marchant DR. 2017. Obliquity-paced climate change recorded in Antarctic debris-covered glaciers. *Nature Communications* **8**: 14194.

Maurer HR, Hauck C. 2007. Instruments and methods – geophysical imaging of alpine rock glaciers. *Journal of Glaciology* **53**: 110–120.

McCarthy M, Pritchard H, Willis I, King E. 2017. Ground-penetrating radar measurements of debris thickness on Lirung Glacier, Nepal. *Journal of Glaciology* **63**: 543–555.

Merz K, Maurer HR, Buchli T, Horstmeyer H, Green AG, Springman SM. 2015. Evaluation of ground-based and helicopter ground-penetrating radar data acquired across an alpine rock glacier. *Permafrost and Periglacial Processes* **26**: 13–27.

Monaghan AJ, Bromwich DH, Wang SH. 2006. Recent trends in Antarctic snow accumulation from Polar MM5. *Philosophical Transactions of the Royal Society A - Mathematical Physical and Engineering Sciences* **364**: 1683–1708.

Monnier S, Kinnard C. 2013. Internal structure and composition of a rock glacier in the Andes (upper Choapa valley Chile) using borehole information and ground-penetrating radar. *Annals of Glaciology* **54**: 61–72.

Monnier S, Kinnard C. 2015. Internal structure and composition of a rock glacier in the dry Andes inferred from ground-penetrating radar data and its artefacts. *Permafrost and Periglacial Processes* **26**: 335–346.

Monnier S, Camerlynck C, Rejiba F. 2008. Ground penetrating radar survey and stratigraphic interpretation of the Plan du Lac rock glaciers Vanoise Massif Northern French Alps. *Permafrost and Periglacial Processes* **19**: 19–30.

Moorman BJ, Robinson SD, Burgess MM. 2003. Imaging periglacial conditions with ground-penetrating radar. *Permafrost and Periglacial Processes* **14**: 319–329.

Orombelli G, Baroni C, Denton GH. 1990. Late Cenozoic glacial history of the Terra Nova Bay region Northern Victoria Land Antarctica. *Geografia Fisica e Dinamica Quaternaria* **13**: 139–163.

Plewes L, Hubbard B. 2001. A review of the use of radio-echo sounding in glaciology. *Progress in Physical Geography* **25**: 203–236.

Ribolini A, Chelli A, Guglielmin M, Pappalardo M. 2007. Relationships between glacier and rock glacier in the Maritime Alps Schiantala Valley Italy. *Quaternary Research* **68**: 353–363.

Ribolini A, Guglielmin M, Fabre D, Bodin X, Marchisio M, Sartini S, Spagnolo M, Schoeneich P. 2010. The internal structure of rock glaciers and recently deglaciated slopes as revealed by geoelectrical tomography: insights on permafrost and recent glacial evolution in the Central and Western Alps (Italy–France). *Quaternary Science Reviews* **29**: 507–521.

Sattler K, Anderson B, Mackintosh A, Norton K, de Róiste M. 2016. Estimating permafrost distribution in the maritime southern Alps New Zealand based on climatic conditions at Rock Glacier sites. *Frontiers in Earth Science* **4**: 1–17.

Seppi R, Carton A, Zumiani M, Dall'Amico M, Zampedri G, Rigon R. 2012. Inventory distribution and topographic features of rock glaciers in the southern region of the eastern Italian Alps (Trentino). *Geografia Fisica e Dinamica Quaternaria* **35**: 185–197.

Serrano E, López-Martínez J. 2000. Rock glaciers in the South Shetland Islands western Antarctica. *Geomorphology* **35**: 145–162.

Shur Y, Hinkel KM, Nelson FE. 2005. The transient layer: implications for geocryology and climate-change science. *Permafrost and Periglacial Processes* **16**: 5–17.

Silva Busso A, Yermolin Y. 2017. Características geológico-geotécnicas y propuestas para la preservación del Sitio y Monumento Histórico n° 38, Cabaña de Nordenskjöld, Antártida. *Boletín Geológico y Minero* **128**: 207–220.

Strelin JA, Sone T. 1998. Rock glaciers on James Ross Island Antarctica. In *Proceedings of the 7th International Permafrost Conference 23–27 June 1998 Yellowknife N.W.T. Canada*, Lewkowicz AG, Allard M (eds). Laval, Centre d'Etudes Nordiques Universite´: Laval; 1027–1032.

Swanger KM, Marchant DR, Kowalewski DE, Head JW, III. 2010. Viscous flow lobes in central Taylor Valley Antarctica: origin as remnant buried glacial ice. *Geomorphology* **120**: 174–185.

Turner J, Barrand NE, Bracegirdle TJ, Convey P, Hodgson DA, Jarvis M, Jenkins A, Marshall G, Meredith MP, Roscoe H, Shanklin J, French J, Goosse H, Guglielmin M, Gutt J, Jacobs S, Kennicutt MC, Masson-Delmotte V, Mayewski P, Navarro F, Robinson S, Scambos T, Sparrow M, Summerhayes C, Speer K, Klepikov A. 2014. Antarctic climate change and the environment: an update. *Polar Record* **50**: 237–259.

Vieira G, Bockheim J, Guglielmin M, Balks B, Abramov AA, Boelhouwers J, Cannone N, Ganzert L, Gilichinsky DA, Goryachkin S, Lopez-Martınez J, Meiklejohn I, Raffi R, Ramos M, Schaefer C, Serrano E, Simas F, Sletten R, Wagner D. 2010. Thermal state of permafrost and active-layer monitoring in the Antarctic: advances during the international polar year 2007–2009. *Permafrost and Periglacial Processes* **21**: 182–197.

Vieira R, Hinata S, da Rosa KK, Zilberstein S, Simoes JC. 2012. Periglacial features in Patriot Hills Ellsworth Mountains Antarctica. *Geomorphology* **155–156**: 96–101.

Wahrhaftig C, Cox A. 1959. Rock glaciers in the Alaska Range. *Geological Society of America Bulletin* **70**: 383–436.

Yoshikawa K, Leuschen A, Ikeda Harada K, Gogineni P, Hoekstra P, Hinzman L, Sawada Y, Matsuoka N. 2006. Comparison of geophysical investigations for detection of massive ground ice (pingo ice). *Journal of Geophysical Research* **111**: E06S19.

Zhao W, Forte E, Colucci RR, Pipan M. 2016. High-resolution glacier imaging and characterization by means of GPR attribute analysis. *Geophysical Journal International* **206**: 1366–1374.